Available online at www.sciencedirect.com
SCIENCE DIRECT
Thermochimica Acta 443 (2006) 235–244
thermochimica acta
www.elsevier.com/locate/tca

Crystallisation, melting, recrystallisation and polymorphism of *n*-eicosane for application as a phase change material

A. Genovese, G. Amarasinghe, M. Glewis, D. Mainwaring, Robert A. Shanks *

School of Applied Science, RMIT University, G.P.O. Box 2476V, Melbourne, Vic. 3001, Australia

Received 2 December 2005; received in revised form 25 January 2006; accepted 3 February 2006

Abstract

Phase change materials (PCM) provide thermoregulation originating from the latent heat exchanged during melting or crystallisation. Linear hydrocarbons have weak interactions, but high symmetry, providing an effective quantity of latent heat over the most acceptable temperature range for applications. The ability to both melt and crystallise over a narrow range is made complex by nucleation, polymorphism and the kinetic nature of these changes. Differential scanning calorimetry (DSC), optical microscopy and temperature modulated DSC (TMDSC) was used to study the melting of *n*-eicosane. This PCM has a low degree of supercooling and conversion to the most stable crystalline state (triclinic) that occurs rapidly from a metastable phase (rotator) state on cooling. TMDSC revealed a small, yet similar degree of thermodynamic reversibility in the melting of each of the crystalline phases.

Keywords: *n*-Eicosane; Phase change material; Melting; Crystallisation; TMDSC

1. Introduction

Phase change materials (PCM) are a favourable media for thermoregulation provided by the latent heat exchanged during a solid–solid, solid–liquid or solid–gas phase change. The selection of a PCM material is dependent on the application temperature as well as the extent of latent heat to be exchanged [1–3]. Phase transition temperatures close to the application temperatures are considered optimal for most thermal energy storage systems with the transition, ideally having a high enthalpy [4]. The two main classes of materials used as latent heat thermal energy storage systems are inorganic compounds, such as salt hydrates [5] and organic compounds, such as alkanes [6–10] and short chain fatty acids [11–13].

Alkane hydrocarbon waxes are principally mixtures of linear chain alkanes ($CH_3(CH_2)_nCH_3$). The methylene segments of the linear alkanes are capable of crystallisation induced by their high symmetry and weak van der Waals interactions. In general, the melting temperature and latent heat increase with increasing chain length. Alkanes display little or no degree of supercooling, crystallisation and melting occurring over narrow temperature ranges. Alkanes provide relatively high latent heat and have significant other characteristics suitable for their application as PCM, being chemically non-aggressive, non-toxic, non-corrosive and possessing long-term stability [7,14].

The physical properties of a homologous series of *n*-alkanes (C_nH_{2n+2}) are sensitive to the number of carbons comprising the chain. An odd-even effect in their melting temperature and latent heat is notable for short chain alkanes, particularly for $C_n \leq 40$ [7]. Various crystal polymorphic structures are formed by various alkanes. The stable low temperature phase is typically the triclinic or orthorhombic crystalline structure for short chain alkanes, although monoclinic and hexagonal structures have also been observed [8,15,16]. The crystalline structure is influenced by a unique mesophase observed in some alkanes. This mesophase, termed the plastic crystalline or rotator phase, occurs in a narrow temperature range although several rotator phases may exist between the crystalline phase and the isotropic liquid state [17].

There have been limited studies focusing on the melting behaviour of small molecules and olefins using temperature modulated differential scanning calorimetry (TMDSC). Longer chain alkanes have received attention as model compounds for an understanding crystallisation and melting behaviour of

* Corresponding author. Tel.: +61 3 9925 2122; fax: +61 3 9369 1321.
E-mail address: robert.shanks@rmit.edu.au (R.A. Shanks).

0040-6031/$ – see front matter © 2006 Elsevier B.V. All rights reserved.
doi:10.1016/j.tca.2006.02.008

macromolecules, particularly polyethylene. The smaller model compounds range from *n*-hexacosane ($C_{26}H_{54}$) to *n*-hexacotane ($C_{60}H_{122}$) [18–20]. Here we extend the use of TMDSC to investigate the melting behaviour of *n*-eicosane. The change in microstructural type (triclinic and rotator phase of *n*-eicosane) was established to identify the influence of the phase state formed during cooling on the metastability, reversibility of the melting transition using TMDSC in the heating and also quasi-isothermal modes. We evaluate these thermal characteristics in terms of the requirements of PCM materials for thermoregulation.

2. Experimental

2.1. Materials

Normal eicosane was obtained from Aldrich Chemical Co., USA with purity greater than 99 mol% and used as received. *n*-Eicosane composition was determined by gas chromatography coupled with mass spectroscopy (GCMS) with a Hewlett Packard 5890 GC and 5970 Series Mass Selective detector. A SGE 30 m × 0.25 mm ID-BPX5 with 0.25 μm film thickness non-polar column was used. The *n*-eicosane was melted and a small volume (1 μL) was injected into the GC with inlet at 40 °C, followed by a temperature ramp of 10 °C min^{-1}. Trace amounts of alkanes (C_{18}, C_{19}) were determined by GCMS, and the results confirmed the purity indicated.

2.2. Calorimetric experiments

A Perkin-Elmer Pyris 1 DSC equipped with an Intracooler 2P cooling facility was used for determining crystallisation and melting properties. The experiments were conducted under a nitrogen purge with a flow rate of 20 mL min^{-1}. The instrument was calibrated for temperature with high purity decane (−56.8 °C), indium (156.60 °C, 28.45 J g^{-1}) and zinc (419.47 °C) standards utilising the onset of each melting transition peak. The onset temperature was determined by extrapolation of the linear portion of the transition to the baseline. The heat flow rate was calibrated with the melting enthalpy of indium. Small sample masses of *n*-eicosane (1.5–2 mg) were accurately weighed using a Perkin-Elmer microbalance (AD–2Z Autobalance) calibrated with a standard 2.000 mg mass. The small masses ensure good contact and control of temperature throughout the sample. The samples were encapsulated in standard hermetically sealed 10 μL aluminium pans and matched empty pans were used as a reference and baseline pans. No mass loss was observed after the calorimetric analysis.

The crystallisation and melting scans of *n*-eicosane were obtained at slow scanning rates of 1 and 2 °C min^{-1} from −20 to 50 °C. Isothermal crystallisation of *n*-eicosane was performed at various temperatures inclusive of 36.5–34.7 °C. Initially *n*-eicosane was completely melted at 45 °C and held for 1 min to destroy thermal history and remove self seeding nuclei prior to rapid cooling to a selected temperature for 14 min, at a specific rate to not overshoot the isothermal crystallisation temperature. The exothermic heat flow over time was recorded in addition to the immediately obtained subsequent melting endotherm (scan rate of 2 °C min^{-1}). Baselines for scans were obtained over the same ranges for the respective melting or crystallisation curves. The kinetics of isothermal crystallisation from the melt was analysed on the basis of the Avrami equation [21–24]. The relative degree of crystallinity, χ_t, is related to the crystallisation time, t, as described by:

$$\chi_t = 1 - \exp(-K(T)t^n) \tag{1}$$

where χ_t is the relative degree of crystallinity, $K(T)$ is a growth function that is dependent on the nucleation and crystal growth and n is the Avrami exponent. The Avrami parameters can be determined from the following rearrangement:

$$\ln[-\ln(1-\chi_t)] = \ln K(T) + n \ln t \tag{2}$$

From a double natural logarithmic plot of $\ln[-\ln(1-\chi_t)]$ versus $\ln t$, n and $K(T)$ are determined from the slope and intercept, respectively, using the linear part of the curves. The crystallisation half time, $t_{1/2}$, is defined as the time at which χ_t is 0.50. It can be calculated from the following expression:

$$t_{1/2} = \left(\frac{\ln 2}{K(T)}\right)^{1/n} \tag{3}$$

Temperature modulated heating scans were conducted utilising a sawtooth modulation (heat-cool profile) superimposed on a linear heating scan on the Perkin-Elmer Pyris 1 DSC. The modulation parameters comprise an underlying heat rate (β_0) of 0.10 °C min^{-1}, temperature amplitude (T_a) 0.15 °C and period (p) of 120 s (frequency 8.3 mHz). The thermal histories imposed on *n*-eicosane were: (i) complete melting as previously described followed by cooling at a scan rate of 1 °C min^{-1} to 30.0 °C, (ii) complete melting, followed by rapid cooling to 35.5 °C and then held isothermally for 12 min. A baseline scan was obtained prior each to thermal treatment. After the selected imposed thermal history, *n*-eicosane was subjected to a temperature modulated scan directly from the end temperature of the treatment, i.e., 30 and 35.5 °C, respectively. In addition, a temperature modulated scan with profile $\beta_0 = 1$ °C min^{-1}, $T_a = 2.35$ °C and $p = 90$ s was also obtained for *n*-eicosane with a thermal history (i). The measured heat flow data was then used to calculate the total heat capacity (total C_p considered to be equivalent to conventional DSC curve) and the reversing (in-phase, C'_p) heat capacity. The non-reversing (C_{pNR}) was obtained by subtracting the C'_p from the total C_p curve and is considered to reflect only irreversible phenomena. Exothermic events are revealed in this contribution and may be revealed as an underlying transformation [25,26]. Quasi-isothermal TMDSC, whereby the underlying heating rate is zero, was conducted with $T_a = 0.5$ °C, $p = 60$ s. The measurements were performed at selected temperatures in the melting range of 30–40 °C, using the method described by Ishikiriyama and Wunderlich [27]. The final 10 min of the 20 modulation cycles was used to determine C'_p. Lissajous figures were constructed to monitor the approach to steady state.

2.3. Hot stage optical microscopy

Hot stage optical microscopy was performed with a Nikon Labophot II microscope under polarised light. Images were captured with an attached Nikon Coolpix 5000 digital camera. *n*-Eicosane was placed between a glass slide and cover slip and sealed with silicone sealant. The specimen was placed on an FP82 Mettler hot stage with temperature controller unit FP90 Mettler central processor. The hot stage was calibrated with the melting of benzoic acid ($T_m = 122\,^{\circ}C$). The *n*-eicosane was heated to 40 °C and held isothermally for 1 min prior to cooling at 0.5 °C min^{-1}. Following crystallisation, the melting was observed at same heating rate. Photomicrographs were attained at various temperatures.

3. Results and discussion

3.1. Standard DSC measurement

The specific heat curves for *n*-eicosane melting and crystallisation processes with scan rates of 1 and 2 °C min^{-1} are shown in Fig. 1a and b respectively. A triclinic crystalline structure (*T*) is the stable low temperature crystalline phase of *n*-eicosane, formed at ambient temperature [8,28]. One endothermic peak was observed for the melting transition that occurred at temperature range of 36–38 °C, the broadening observed was attributed to the change in scan rate. The peak melting temperatures occurred at 36.9 and 37.1 ± 0.1 °C for the respective heating rates. The endothermic phase transition has a latent heat of melting (enthalpy) that remained constant at 247.6 ± 0.6 J g^{-1} (69.8 kJ mol^{-1}), comparable with literature (69.9 kJ mol^{-1}) [7,29]. When *n*-eicosane was cooled at 1 °C min^{-1} from the liquid phase (L), solidification commenced at 36.0 °C and concluded at 34.8 °C forming a metastable rotator phase (R_I). A sharp solid–solid transition occurred between 34.0 and 33.8 °C where the rotator phase transformed into a stable triclinic crystalline phase [8].

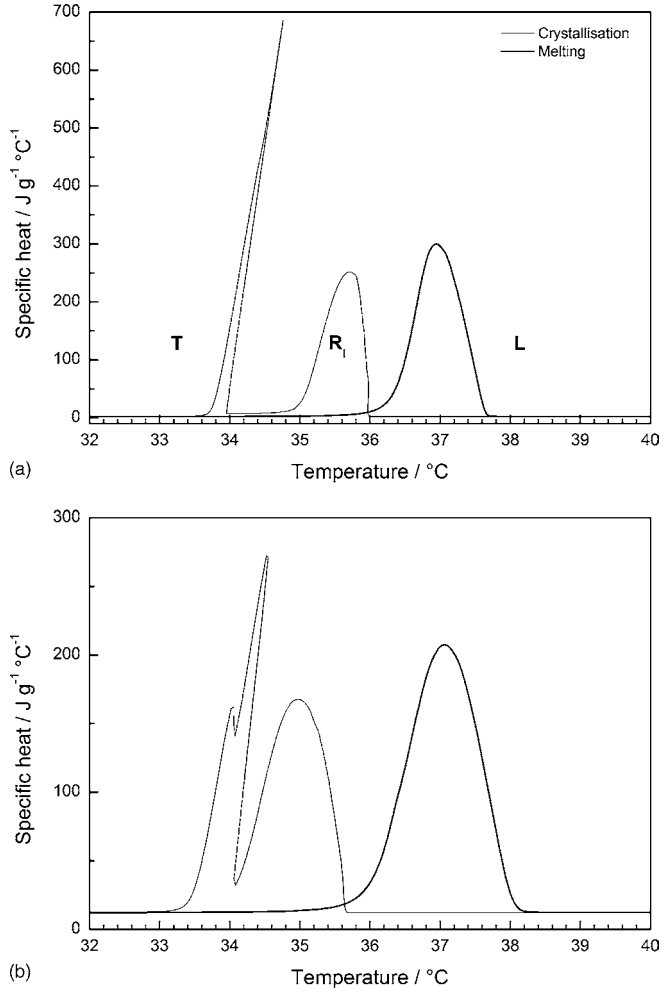

Fig. 1. Specific heat crystallisation and melting curves of *n*-eicosane obtained with scanning rate of: (a) 1 °C min^{-1} and (b) 2 °C min^{-1}.

Similarly, on cooling at 2 °C min^{-1}, the onset of crystallisation was 35.6 °C. The solid–solid transition from the rotator phase to the stable triclinic structure began at 34.0 °C with the appearance of a sharp double exotherm. The transition to the triclinic state was completed by 33.4 °C. The sharp exotherm at the rotator–triclinic phase change was rapid while the DSC sample sensor temperature response was found to increase by ∼0.8 °C, causing the peak to be slanted towards higher temperature, attributed to the heat evolved in the conversion.

The progression of the liquid phase to the rotator phase was indicated by the formation of crystals as seen in Fig. 2a at 35.1 °C. Further cooling resulted in the rapid transformation of the metastable rotator phase to the triclinic crystal structure. This solid–solid transition is seen in consecutive photomicrographs ‘b’ and ‘c’, where this phenomenon occurred within less than 0.1 °C. At 30 °C ‘d’, the structure obtained is the low temperature stable form of *n*-eicosane. The subsequent melting of *n*-eicosane, displayed in the sequence ‘d–f’, shows the disappearance of the crystalline structure and no further evidence of the rotator phase.

The rotator phase is associated with the degrees of freedom within a lamellar crystal, that is, the rotations about the molecule long axis within the crystal whilst maintaining positional order [30–32]. There are five unique mesophases found in alkanes and *n*-eicosane exhibits R_I rotator phase only on cooling. This R_I rotator phase has a rectangular or distorted hexagonal lattice as described in detail by Sirota et al. [6]. Some alkanes display rotator phases on both heating and cooling, particularly the odd carbon numbered alkane sequence from C_9 to C_{21} [8].

The development of crystallinity with time over the temperature range from 36.5 to 34.7 °C (isothermal crystallisation temperature, T_{IC}) was obtained for *n*-eicosane and data given in Table 1. A single relatively broad exothermic peak was observed at temperatures between 36.5 and 35.25 °C. The crystallisation was in the range for the rotator phase formation as seen from previous crystallisation exotherm scans. Fig. 3a shows a typical plot obtained for relative crystallinity versus crystallisation time of *n*-eicosane at an isothermal crystallisation temperature of 35.5 °C. At this temperature, we isolate the formation of the rotator phase in the given crystallisation time. The experimental data was fitted using the Avrami equation. After an initial short induction time for nuclei formation, a rapid increase in

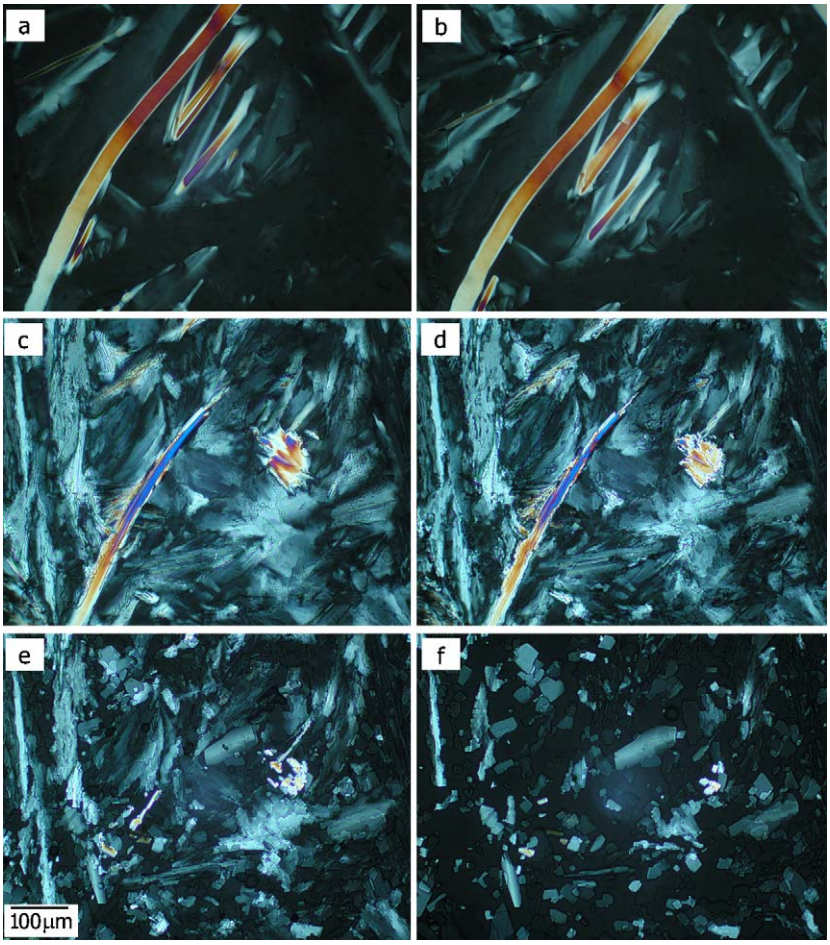

Fig. 2. Polarised optical micrographs of *n*-eicosane (obtained at scan rate of 0.5 °C min^{-1}): (a) formation of metastable rotator phase observed at 35.1 °C, (b and c) rapid solid–solid transformation to triclinic crystal structure (34.7 to 34.6 °C), (d–f) progression of melting of the triclinic crystal structure (30.0, 36.4 and 36.6 °C).

the relative crystallinity is observed before a plateau forms as crystallisation approaches completion. Fig. 3b displays the corresponding Avrami plot of the crystallisation, $\ln[-\ln(1-\chi_t)]$ versus $\ln t$. The evaluation of both n and $K(T)$ were extracted from the early stages of crystallisation in the linear region and the crystallisation half time ($t_{1/2}$) was calculated using Eq. (3).

The $t_{1/2}$ of R_I rapidly decreases with a lowering of crystallisation temperature from 148.9 to 9.9 s as shown in Table 1. The corresponding melting peak appeared at 36.7 °C. The corresponding enthalpy of melting for the rotator phase formation was found to increase with decreasing isothermal crystallisation temperature, indicating greater conversion from the melt. At temperatures of 35.15 and 34.7 °C, formation of the rotator phase occurred with the appearance of a sharp exotherm. R_I $t_{1/2}$ occurred at 9.3 and 5.8 s, respectively. The average value of n for the rotator phase formation was determined to be 1.9, indicating that the rapid simultaneous nucleation and growth was two-dimensional. The crystallisation rate $K(T)$, related to

Table 1
Isothermal crystallisation and corresponding melting properties of *n*-eicosane

T_{IC} (°C)	R_I $t_{1/2}$ (s)	k ($\times 10^{-3}$ min^{-n})	Melting phase	Corresponding T_m (°C)	ΔH_m (J g^{-1})
36.5	148.9	$0.15R_I$	Rotator	36.7	123.7
36.3	41.8	$0.73R_I$	Rotator	36.7	153.4
36.15	28.2	$1.05R_I$	Rotator	36.7	158.4
36	20.1	$1.36R_I$	Rotator	36.7	161.4
35.75	14.4	$2.42R_I$	Rotator	36.7	164.1
35.5	11.5	$7.01R_I$	Rotator	36.7	166.5
35.25	9.9	$9.43R_I$	Triclinic	Conversion R_I to T at start of scan, 37.0	168.9
35.15	$9.3R_I$ $10.8T$	$9.78R_I$ $3.33T$	Triclinic	37.0	244.6
34.7	–	–	Triclinic	37.0	244.9

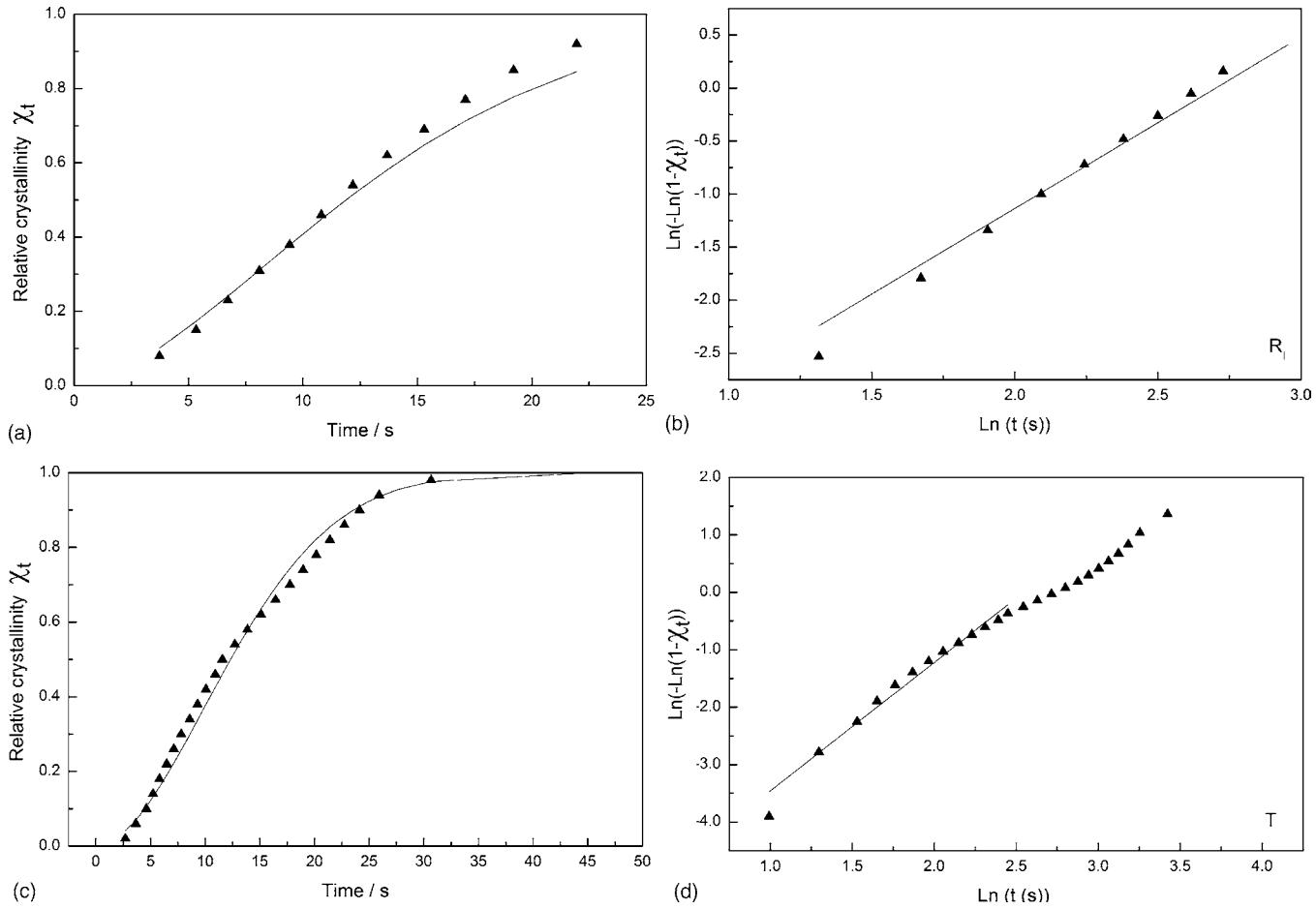

Fig. 3. Isothermal crystallisation of *n*-eicosane, development of the relative degree of crystallisation with time for (a) rotator phase (R_I) and (c) triclinic crystal structure (T). Corresponding plot of $\ln[-\ln(1-\chi_t)]$ vs. $\ln t$ for (b) R_I at 35.5 °C and (d) T at 35.15 °C.

the mechanism of nucleation and crystal growth, increased as a function of decreasing temperature from 0.15×10^{-3} to $9.78 \times 10^{-3}\,\mathrm{min}^{-n}$.

After a short time of holding the *n*-eicosane isothermally (~96 s) at 35.15 °C, an exotherm appeared indicating the formation of the more thermally stable triclinic phase. The corresponding melting peak was at 37.0 °C, as seen previously for the continually cooled *n*-eicosane. Crystallisation at 34.7 °C resulted in formation of the rotator phase and subsequent triclinic phase conversion in rapid succession resulting in a merging of transitions (R_I peak at 6.8 s, T peak at 17.4 s), leaving no time for baseline heat flow to be obtained. The subsequent melting showed a characteristic triclinic melting peak temperature of 37.0 °C. Fig. 3c and d show the Avrami analysis curves for this transformation. The development over time was linear at early conversion. Deviation from linearity may be attributed to the solid–solid phase transformation since typically isothermal crystallisation is obtained from a melt. At low conversion, n was 2.2, suggesting that the existing crystalline regions can nucleate the remaining uncrystallised *n*-eicosane, as the melting enthalpy indicates ($244.6\,\mathrm{J\,g}^{-1}$). Kraack et al. have indicated that nucleation can indeed proceed through a transient metastable rotator phase, as has been found for various alkanes [33,34]. Crystallisation half time was 10.8 s and $K(T)$ was slower ($3.33 \times 10^{-3}\,\mathrm{min}^{-n}$) than the rotator phase rate for the same isothermal crystallisation temperature.

3.2. Temperature modulated DSC measurement

The melting transition of the stable triclinic phase of *n*-eicosane was further analysed by TMDSC. Fig. 4 shows the heat capacity curves obtained for *n*-eicosane cooled continuously at $2\,^{\circ}\mathrm{C\,min}^{-1}$. The underlying heating rate used was $0.10\,^{\circ}\mathrm{C\,min}^{-1}$ to enable processes to closely follow the temperature modulation. Several heat capacity curves can be obtained from the raw heat flow data. The total heat capacity curve (C_{pT}) is similar to conventional DSC, however under modulated temperature conditions, the melting endotherm appeared significantly narrower. The melting peak and enthalpy were similar at 36.7 °C and $247.7\,\mathrm{J\,g}^{-1}$, respectively. The reversing heat capacity curve shows *n*-eicosane exhibiting a reversing melting contribution throughout the central part of melting region where the melting rate was a maximum. This can occur since there was still unmelted *n*-eicosane that can nucleate in the local vicinity of a crystal. The reversing component of the total heat capacity represents effects that are thermodynamically reversible at the time and temperature at which they are detected, i.e., the in-phase response that is capable of following the temperature modula-

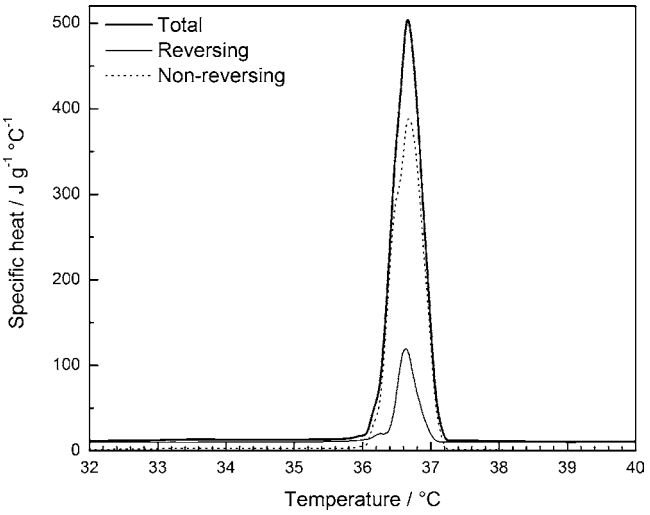

Fig. 4. Temperature modulated specific heat melting curves of *n*-eicosane from the triclinic crystal structure. *Modulation profile*: $\beta_0 = 0.1\,^{\circ}\mathrm{C\,min^{-1}}$, $T_a = 0.15\,^{\circ}\mathrm{C}$ and $p = 120\,\mathrm{s}$.

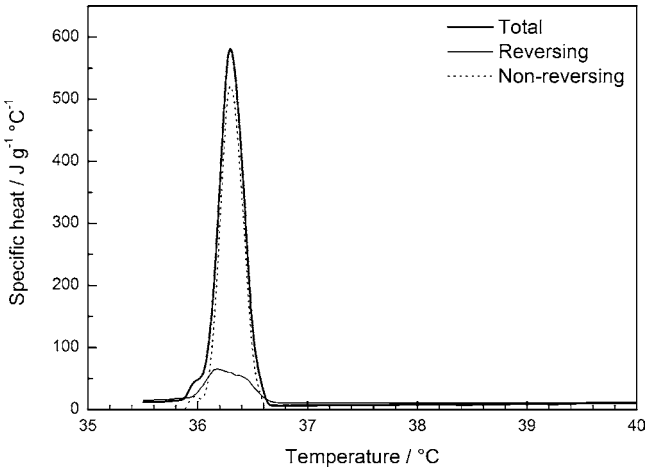

Fig. 5. Temperature modulated specific heat melting curves of *n*-eicosane isothermally crystallised at 35.5 °C, melting from the metastable rotator crystal phase. *Modulation profile*: $\beta_0 = 0.1\,^{\circ}\mathrm{C\,min^{-1}}$, $T_a = 0.15\,^{\circ}\mathrm{C}$ and $p = 120\,\mathrm{s}$.

tion. Some of the reversing contribution may arise from slower processes that have not reached equilibrium. The non-reversing (NR) contribution to the melting represents all irreversible events of the total heat capacity at the time and temperature of the event. Such thermal events are not in-phase with the modulation temperature. The non-reversing heat capacity (C_{pNR}) of *n*-eicosane indicated that irreversible melting was the dominant process. Any exothermic processes that form part of the non-reversing contribution that may have occurred, would be offset by melting. The NR melting enthalpy was $208.9\,\mathrm{J\,g^{-1}}$, as listed in Table 2.

The isothermal crystallisation of *n*-eicosane has demonstrated that we can isolate the melting behaviour of the triclinic and the rotator phase. We can use this by specifically crystallising *n*-eicosane into the rotator phase and applying TMDSC to investigate the corresponding melting transition of this phase. *n*-Eicosane was crystallised at 35.5 °C and the corresponding melting analysed directly from the isothermal crystallisation temperature. Fig. 5 presents the temperature modulated curves for the rotator phase. The total heat capacity curve is sharp and narrower than the melting of the triclinic phase previously observed, attributed to the metastability of the rotator phase. The melting peak and enthalpy was 36.3 °C and $159.5\,\mathrm{J\,g^{-1}}$, respectively, both are marginally lower than those obtained by conventional melting. This phase was observed to exhibit a reversing contribution to the melting transition. The reversing heat capacity curve spans the range of melting observed in the total heat capacity curve with the peak shifted towards the lower temperature side of the endotherm (36.2 °C). This contribution indicates that this phase of *n*-eicosane melted reversibly at the interface of the crystals. It follows that as temperature increases, the melting process dominates as seen in the non-reversing heat capacity curve, and the amount of reversible melting decreases until no further nucleating surfaces are present. The irreversible melting curve was significant with an enthalpy of $123.7\,\mathrm{J\,g^{-1}}$.

Both the triclinic and rotator phases have shown a comparable reversing contribution to the total heat capacity enthalpy ($T \sim 15.9\%$, $R_I \sim 15.1\%$), which is reinforced by their similar structure. That is, the triclinic phase is the stable crystalline phase while the rotator phase has an increased degree of freedom about the long axis of the molecule as previously mentioned. In both cases, the reversible melting can occur well into the melting range of *n*-eicosane. TMDSC has given insight into the reversibility of the phases that otherwise would not have been obtained.

The effect of temperature amplitude (T_a) is a considerable factor in the application of *n*-eicosane as a phase change material. In the TMDSC curves, the amplitude was 0.15 °C in order to maintain small fluctuations in temperature over the modulation period (120 s). This is important since *n*-eicosane has a narrow melting and crystallisation temperature range. The degree of supercooling, as noted from Fig. 1, is less than 2 °C for the scan rates used between the peak of the melting of triclinic phase and the peak of the rotator phase formation. Fig. 6 demonstrates the effect of large temperature amplitude. The amplitude was 2.35 °C which principally causes a dramatic fluctuation in temperature experi-

Table 2
TMDSC melting properties of the triclinic crystalline phase and metastable rotator phase

Treatment	Total C_p		Reversing C_p		Non-reversing C_p	
	T_m (°C)	ΔH_m (J g^{-1})	T_m (°C)	ΔH_m (J g^{-1})	T_m (°C)	ΔH_m (J g^{-1})
(i) Crystallisation to triclinic phase	36.7	247.7	36.6	39.3	36.6	208.9
(ii) Isothermal crystallisation at 35.5 °C	36.3	159.5	36.2	24.2	36.3	123.7

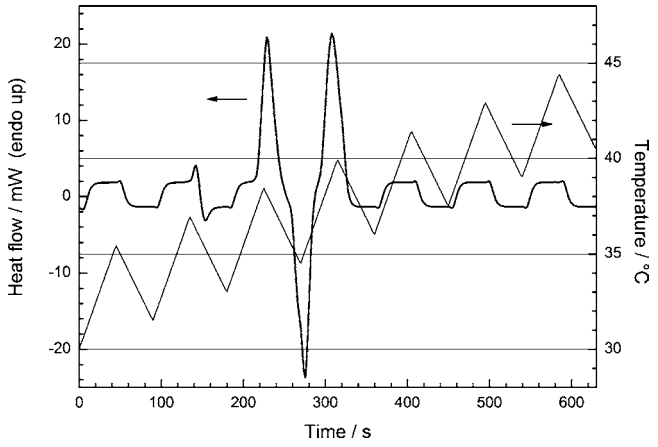

Fig. 6. Modulated heat flow (bold line) over temperature domain and sawtooth temperature profile (thin line). Large temperature amplitude effect on the melting and crystallisation of *n*-eicosane. *Modulation profile*: $\beta_0 = 1.0\,^{\circ}\mathrm{C\,min^{-1}}$, $T_a = 2.35\,^{\circ}\mathrm{C}$ and $p = 90$ s.

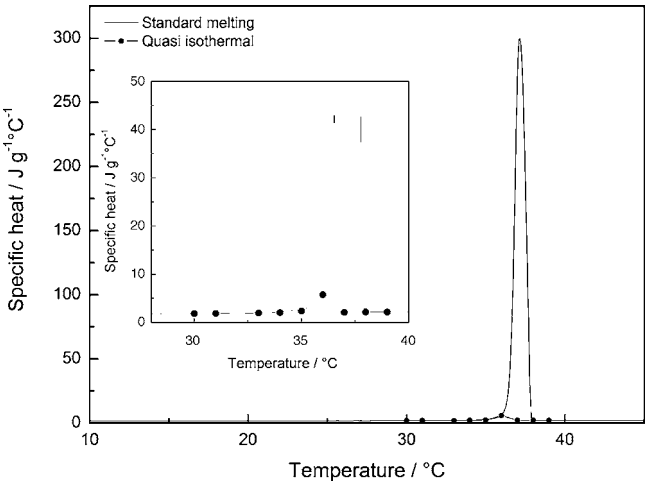

Fig. 7. Quasi-isothermal reversing specific heat of *n*-eicosane, where the line indicates standard DSC melting endotherm at a scanning rate of $1\,^{\circ}\mathrm{C\,min^{-1}}$. Quasi-isotherm measurements (filled circles) obtained with profile $\beta_0 = 0\,^{\circ}\mathrm{C\,min^{-1}}$, $T_a = 0.5\,^{\circ}\mathrm{C}$ and $p = 60$ s.

enced by *n*-eicosane. The heat-cool temperature profile and heat flow over time is shown. From this profile, a particular temperature is passed through rapidly multiple times. The heat flow response shows three endothermic peaks that occur during the heating segments of the modulation cycle and three exothermic peaks that occur during the cooling segments. The fluctuations cause rapid changes in *n*-eicosane crystallisation and melting behaviour. It is possible that the extreme changes in temperature may cause formation of the rotator phase on cooling that may contribute to the melting in the next cycle. With the underlying temperature gradually increasing, the relative amount of conversion to the triclinic phase would decrease with the cooling experienced. Meanwhile, there would be a lower rate of conversion to the rotator phase within the modulation cycle. Hence, the melting behaviour is made complex by the close proximity of the melting, crystallisation and solid–solid transformations. This infers that to maintain the PCM performance of *n*-eicosane in applications, it is preferable to cool to lower temperatures for complete solid–solid transformation. This would ensure greater enthalpy for the absorption of heat from the triclinic phase to the melting phase under appropriate operating conditions.

Quasi-isothermal (QI) TMDSC analysis allows the investigation of truly reversible events under a modulation profile with no net increase or decrease in temperature. The quasi-isothermal specific heat curve of *n*-eicosane over selected temperatures between 30 and 39 °C is shown in Fig. 7. A number of modulation cycles are required before steady state can be reached. In the first few modulation cycles at a particular temperature, both irreversible and reversible events occur while the former can cause distortion in the reversible melting response. Once the distortions are removed and steady state is approached, the truly reversing contribution can be obtained. Steady state was monitored through the construction of Lissajous figures (Fig. 8). As shown in Fig. 7, the measurements (filled circles) indicate that *n*-eicosane exhibits a truly reversible melting contribution, although the contribution is relatively low (∼2%) in comparison with the total heat capacity curve. From the reversing specific heat over time, the heat capacity increased marginally with temperature between 30 and 34 °C. At 35 °C, it increased slightly as more of the *n*-eicosane melted and recrystallised in the presence of a nucleating surface. At 36 °C, reversible melting was observed and steady state maintained throughout all the modulation cycles. However, at 37 °C, a rapid change occurred. Within the first modulation cycle, a significant decrease in the reversing heat capacity in the melting part of the modulation indicates that melting is dominant prior to any crystallisation. After complete melting, attainment of steady state was regained. The corresponding Lissajous figures with normalised heat flow are shown in Fig. 8 demonstrating that a steady state is maintained at all temperatures, indicated by the overlapping Lissajous loops. Only at 36 °C is there a change in the envelope shape due to the reversible melting active at this temperature. Once completely melted, the envelope indicates steady state is reached in the melt.

n-Eicosane has a low melting temperature appropriate for use as a PCM for thermoregulation in human physiological applications. The thermal properties including latent heat are important considerations that rely on the formation and loss of weak van der Waals forces that maintain the crystalline structure. On cooling from the melt, a low degree of supercooling is characterised by the ease of molecular segments aggregating to form a stable nucleus. With little or no supercooling, the van der Waals interactions between the converging chains result in the formation of an ordered structural arrangement. The particular metastable rotator and stable triclinic phases can be analysed using X-ray techniques such as those applied to *n*-hexatricotane ($C_{36}H_{74}$) by Dorset [35]. The crystallisation is rapid and alkanes are known to form various macromorphological structures, for example, platelets and needles [9] although these are made complex by various time, temperature and rate factors. *n*-Eicosane forms an extended chain crystal structure [34,36], that has implications in the melting behaviour as well as its reversing and thermodynamically reversible melt-

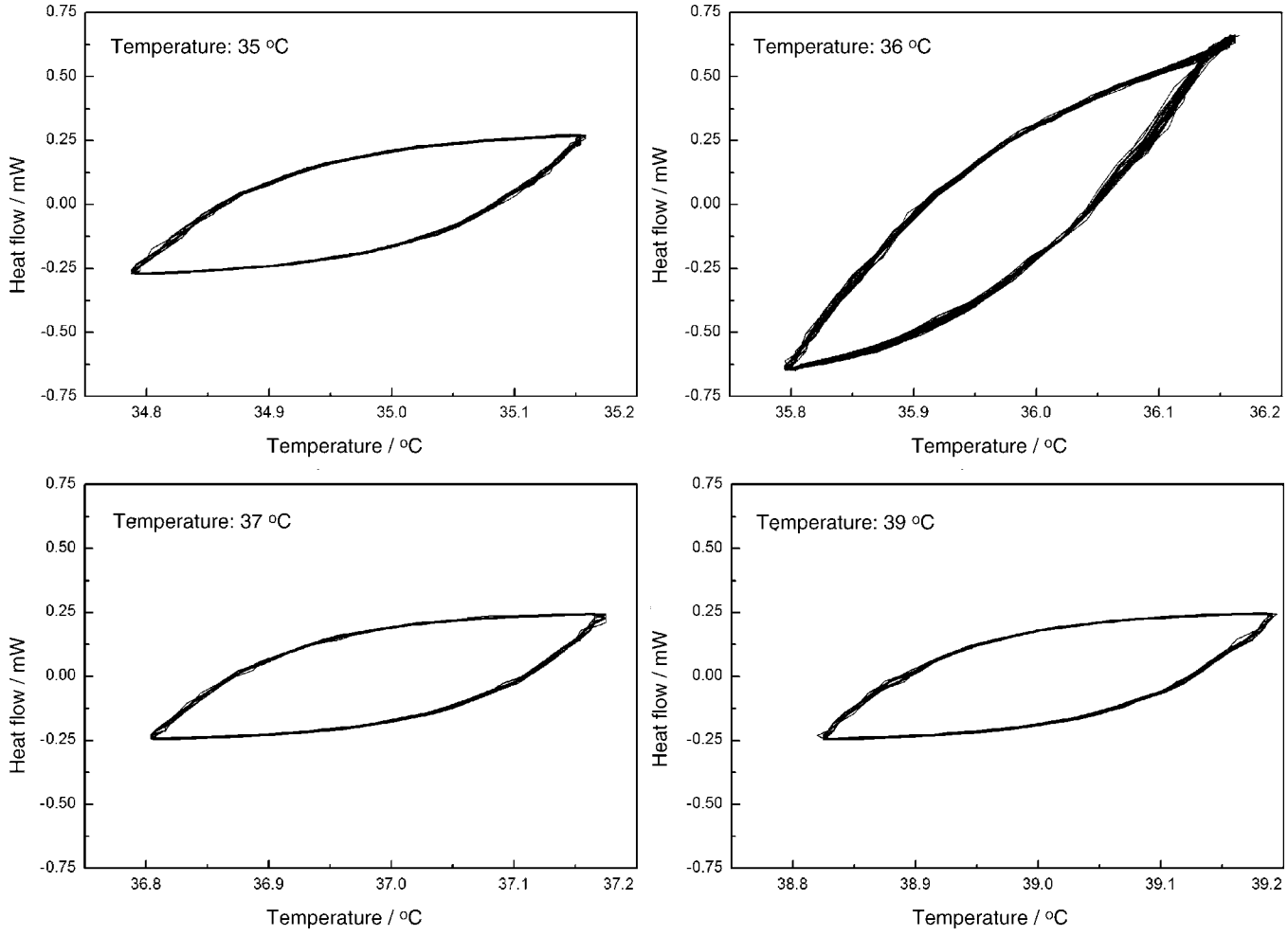

Fig. 8. Lissajous figures obtained from the reversing specific heat curves at the specified temperatures indicated.

ing contributions. This has been observed in this study and is supported by measurements on slightly longer alkanes, including *n*-hexacosane ($C_{26}H_{54}$), pentacontane and hexacontane that also have shown a largely reversible melting contribution that extends well into the melting range of the particular alkane [20,36,37]. Notably, reversible melting behaviour is attributed to the mobility of the alkane at the localised interface of the crystal. The crystalline structure typically changes with increasing molar mass from an extended chain crystal through to a chain folded crystallite structure (as formed in polyethylene). The reversibility in the melting of chain folded crystallites involves the uncrystallised segments of a molecule that are anchored by the remaining portion of the molecule in the lamellae component. This process requires energy barriers to be reduced and unravelling of the random coil configuration before reattachment to the lamellae surface. A requirement for molecular nucleation in the long alkanes is important in reversible melting. Once molecules have detached from the lamellae surface and entered the melt, large supercooling is required for nucleation. *n*-Eicosane may possess higher thermal mobility and a lack of anchorage to a crystal given the small molecule length and surface energy factors that affects its crystallisation properties [34].

The immediate microclimate temperature and associated fluctuations of the PCM will dictate the range over which the heat exchange or transfer will occur, for instance, thermoregulation from a body to the PCM. For effectiveness in heat transfer applications adapted for the human body, the PCM operating temperature range must be selected to efficiently cool the skin and core body without inducing vasoconstriction, a physiological response to extreme peripheral cooling [38], such as that occurring with the solid-to-liquid transformation of water as a PCM [39–42]. *n*-Eicosane is an alternative to water with the phase transition occurring closer to natural body temperature. When in contact with the skin in suitable containment, heat can be transferred to *n*-eicosane and absorbed to melt the crystals (latent heat) leading to a less dramatic temperature change and more gradual skin cooling sensation. The solid-to-liquid transformation, the transition can be represented by the upper schematic shown in Fig. 9. For regeneration of the PCM in cooling applications, the temperature must decrease sufficiently to enable crystallisation (solidification). While water has a direct transformation to produce a solid (upper schematic) [43–45], *n*-eicosane requires the formation of the metastable rotator phase before complete conversion to the stable triclinic phase, as represented in the lower schematic in Fig. 9. Therefore, optimal

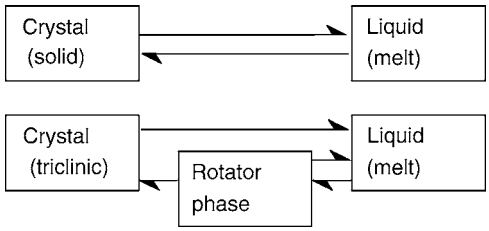

Fig. 9. Direct reversible crystal-liquid equilibrium (top) phase transformation. *n*-Eicosane phase transformation to liquid from the stable triclinic phase. The solidification (crystallisation) to a metastable rotator phase of *n*-eicosane, prior to the solid–solid transformation to the triclinic phase that occurs with a sufficient lowering of temperature. Melting can occur from both phase states (bottom).

performance requires adequate cooling to the stable phase to ensure maximum enthalpy of melting in thermoregulatory operation. If the temperature is reduced to form the intermediate metastable rotator phase, a significant loss of performance will result in the corresponding melting.

4. Conclusion

The scope of this investigation was to explore the thermal behaviour of *n*-eicosane and evaluate its phase change properties. Phase change materials have found widespread use for thermoregulation, although their thermal, physical and chemical behaviour can limit the adaptability towards various applications. The thermal properties that are principally required include the temperature and range of phase transition, degree of supercooling and the associated latent heat of transition. It has been shown that *n*-eicosane can be adapted for use in physiological applications as it possesses attributes particularly suited to the appropriate temperature range. In addition to its narrow melting range, it has a relatively high latent heat of melting ($\sim$247 J g^{-1}) providing adequate PCM efficiency. In order to maintain the level of this efficiency and performance, crystallisation (or regeneration) of the PCM must undergo sufficient cooling to obtain the most stable crystalline form, the triclinic phase. A metastable rotator phase must form prior to undergoing a solid-to-solid transformation to obtain the stable phase. As observed through isothermal crystallisation of *n*-eicosane, a low degree of supercooling reduces the efficiency up to half due to the metastable rotator phase.

Temperature modulated DSC provided further insight into the reversing and non-reversing character of crystallisation and melting. Utilising small temperature amplitude, given that the melting and crystallisation range is narrow, we have observed that both the rotator and triclinic phases exhibited a reversible melting contribution to similar extents. The relative proportion to the overall melting was small ($\sim$15%) and may be attributed to the mobility of the small molecules and lack of anchorage or entanglement that is present in longer alkane chains.

Acknowledgments

Amarasinghe, Glewis and Mainwaring acknowledge the Australian Research Council and the Australian Institute of Sport for funding of this project. We thank Parwin Zaher for assistance in conducting the gas chromatography mass spectroscopy. We are also grateful to the reviewers for drawing our attention to further related literature.

References

[1] U. Beginn, Macromol. Mater. Eng. 288 (2003) 245.
[2] A. Abhat, Solar Energy 30 (1983) 313.
[3] S.M. Hasnain, Energy Convers. Manag. 39 (1998) 1127.
[4] M. Xiao, B. Feng, K. Gong, Energy Convers. Manag. 43 (2001) 103.
[5] M.M. Farid, A.M. Khudhair, S.A.K. Razack, S. Al-Hallaj, Energy Convers. Manag. 45 (2004) 1597.
[6] E.B. Sirota, H.E. King Jr., H.H. Shao, D.M. Singer, J. Phys. Chem. 99 (1995) 798.
[7] S. Himran, A. Suwono, G.A. Mansoori, Energy Sources 16 (1994) 117.
[8] P. Espeau, L. Robles, D. Mondieig, Y. Haget, M.A. Cuevas-Diarte, H.A.J. Oonk, J. Chim. Phys. PCB 93 (1996) 1217.
[9] W.R. Turner, Ind. Eng. Chem. Prod. Res. Dev. 10 (1971) 238.
[10] V. Chevallier, M. Bouroukba, D. Petitjean, D. Barth, P. Dupuis, M. Dirand, J. Chem. Eng. Data 46 (2001) 1114.
[11] F.G. Gandolfo, A. Bot, E. Floter, Thermochim. Acta 404 (2003) 9.
[12] A. Hasan, A.A. Sayigh, Renew. Energy 4 (1994) 69.
[13] A. Sari, K. Kaygusuz, Renew. Energy 28 (2003) 939.
[14] H. Bo, E.M. Gustafsson, F. Setterwall, Energy (Oxford) 24 (1999) 1015.
[15] A. Hammami, A.K. Mehrotra, Fuel 74 (1995) 96.
[16] G. Ungar, N. Masic, J. Phys. Chem. 89 (1985) 1036.
[17] S.J. Severtson, M.J. Nowak, Langmuir 18 (2002) 9371.
[18] J. Pak, B. Wunderlich, J. Polym. Sci. Part B: Polym. Phys. 40 (2002) 2219.
[19] J. Pak, B. Wunderlich, J. Polym. Sci. Part B: Polym. Phys. 38 (2000) 2810.
[20] J. Pak, M. Pyda, B. Wunderlich, Thermochim. Acta 396 (2003) 43.
[21] M. Avrami, J. Chem. Phys. 7 (1939) 1103.
[22] K. Nagarajan, K. Levon, A.S. Myerson, J. Therm. Anal. Calorim. 59 (2000) 497.
[23] E.S. De Medeiros, R.S. Tocchetto, L.H. De Carvalho, I.M.G. Santos, A.G. Souza, J. Therm. Anal. Calorim. 66 (2001) 523.
[24] M.J. Jenkins, J.N. Hay, J. Therm. Anal. Calorim. 56 (1999) 1081.
[25] G. Amarasinghe, F. Chen, A. Genovese, R.A. Shanks, J. Appl. Polym. Sci. 90 (2003) 681.
[26] A. Genovese, R.A. Shanks, J. Therm. Anal. Calorim. 75 (2004) 233.
[27] K. Ishikiriyama, B. Wunderlich, J. Polym. Sci. Part B: Polym. Phys. 35 (1997) 1877.
[28] J.M. Crissman, E. Passaglia, R.K. Eby, J.P. Colson, J. Appl. Crystallogr. 3 (1970) 194.
[29] A. Wurflinger, L.C. Pardo, Z. Naturforsch. A: Phys. Sci. 57 (2002) 177.
[30] G. Ungar, J. Phys. Chem. 87 (1983) 689.
[31] E.B. Sirota, H.E. King Jr., D.M. Singer, H.H. Shao, J. Chem. Phys. 98 (1993) 5809.
[32] E.B. Sirota, Langmuir 14 (1998) 3133.
[33] H. Kraack, E.B. Sirota, M. Deutsch, J. Chem. Phys. 112 (2000) 6873.
[34] H. Kraack, M. Deutsch, E.B. Sirota, Macromolecules 33 (2000) 6174.
[35] D.L. Dorset, J. Electron. Microsc. 2 (1985) 89.
[36] J. Pak, B. Wunderlich, Macromolecules 34 (2001) 4492.
[37] B. Wunderlich, Thermochim. Acta 396 (2003) 33.
[38] R. Lenhardt, Best Pract. Res. Cl Anaesthiol. 17 (2003) 569.
[39] S.Á. Arngrïmsson, D.S. Petitt, M.G. Stueck, J. D.K., D.S. Cureton, J. Appl. Physiol. 96 (2003) 1867.
[40] F.E. Marino, Br. J. Sports Med. 36 (2002) 89.

[41] D.T. Martin, A.G. Hahn, R. Ryan-Tanner, K. Yates, H. Lee, J. Smith, Sportscience 2 (1998), sportsci.org/jour/9804/dtm.htm (Accessed 31/07/05).
[42] M.B. Brearley, J.P. Finn, Sportscience 7 (2003), sportsci.org/jour/03/mbb.htm (Accessed 31/07/05).
[43] L. Royon, P. Perrot, G. Guiffant, S. Fraoua, Energy Convers. Manag. 39 (1998) 1529.
[44] L.F. Cabeza, H. Mehling, S. Hiebler, F. Ziegler, Appl. Therm. Eng. 22 (2002) 1141.
[45] L. Royon, G. Guiffant, Energy Convers. Manag. 42 (2001) 2155.